REFERENCES

Abdelkefi, H., Khemakhem, H., Velu, G., Carru, J.C., and Von der Muhll, R. (2005) Dielectric properties and ferroelectric phase transitions in $Ba_xSr_{1-x}TiO_3$ solid solution. Journal of Alloy and Compound, 399, 1-6.

Agag, T. and Takeichi, T. (2000) Polybenzoxazine-montmiorillnonite hybrid nanocomposites: synthesis and characterization. Polymer, 41, 7083-7090.

Arlt, G., Henning, D., and With, G.D. (1985) Dielectric properties of fine grained barium titanate ceramics. Journal of Applied Physics, 58(4), 1619-1625.

Bai, Y., Cheng, Z.Y., Bharti, V., Xu, H.S., and Zhang, Q.M. (2000) High dielectric constant ceramic powder polymer composites. Applied Physics Letters, 76(25), 3804-3806.

Buchanan, R.C. (2004) Ceramic Materials for Electronic. New York: Marcel Dekker.

Cheng, K.C., Lin, C.M., Wang, S.F., Lin, S. T., and Yang, C. F. (2006) Dielectric properties of epoxy resin-barium titanate composites at high frequency Materials Letters, 61(3), 757-760.

Cho, S.D., Lee, J.Y., and Paik, K.W. (2002) Study on the epoxy/$BaTiO_3$ embedded capacitor films newly developed for PWB applications. Electronic Components and Technology Conference Proceeding 52nd, 504-509.

Devaraju, N.G., Kim, E.S., and Lee, B.I. (2005) The synthesis and dielectric study of $BaTiO_3$/polyimide nanocomposite films. Microelectronic Engineering, 82, 71-83.

Dias, C.J., and Das-Gupta, D.K. (1996) Inorganic ceramic/polymer ferroelectric composite electrets. IEEE Transactions on Dielectrics and Electrical Insulation, (5), 706-734.

Deshpande, S.B., Godbole, P.D., Khollam, Y.B., and Potdar, H.S. (2005) Characterization of barium titanate: $BaTiO_3$ (BT) ceramics prepared from sol-gel derived BT powders. Journal of Electroceramics, 15, 103-108.

Damjanovic, D. (1998) Ferroelectric, dielectric and piezoelectric properties of ferroelectric thin films and ceramics. Report on Progress in Physics, 61, 1267-1324.

Fu, C., Yang, C., Chen, H., Wang, Y., and Hu, L. (2005) Microstructure and dielectric properties of $Ba_xSr_{1-x}TiO_3$ ceramics. Materials Science and Engineering B, 119, 185–188.

Giridharan, N.V., Jayavel, R., and Ramasamy, P. (2001) Structural, morphological and electrical studies on barium strontium titanate thin films prepared by sol-gel technique. Crystal Resource Technology, 36(1), 65–72.

Holly, F.W. and Cope, A.C. (1944) Condensation products of aldehydes and ketones with o-aminobenzyl alcohol and o-hydroxybenzyl amine. Journal of American society, 66, 1875.

Hsiang, H.I., Lin, K.Y., Yen, F.S., Hwang C.Y. (2001) Effects of particle size of $BaTiO_3$ powder on the dielectric properties of $BaTiO_3$/polyvinylidene fluoride composites. Journal of Materials, 36, 3809 – 3815.

Hu, T., Jantunen, H., Unsimaki, A., and Leppavuori, S. (2004) BST powder with sol-gel process in tape casting and firing. Journal of the European ceramic society, 24, 1111-1116.

Ishida, H., and Allen, D.J. (1996A) Physical and mechanical characterization of near-zero shrinkage polybenzoxazines. Journal of Polymer Science, 34, 1019- 1030.

Ishida, H., and Rimdusit, S. (1998) Very high thermal conductivity obtained by boron nitride-filled polybenzoxazine. Thermochimica Acta, 320,177-186.

Ishida, H.and Rodriguez, Y. (1995) Curing kinetics of a new benzoxazine-based phenolic resin by differential scanning calorimetry. Polymer, 36(16), 3151-3158.

Kuo, D.H., Chang, C.C., Su, T.Y., Wang, W.W., and Lin, B.Y. (2004) Dielectric properties of three ceramic/epoxy composites. Material Chemistry and Physics, 85, 201-206.

Kareiva, A., Tautkus, S., Rapalaviciute, R., Jorgensen, J.E., and Lundtof, B. (1999) Sol-gel synthesis and characterization of barium titanate powder. Journal of Materials Science, 34, 4853-4857.

Kuo, D.H., Chang, C.C., Su, T.Y., Wang, W.W., and Lin, B.Y. (2001) Dielectric behaviours of multi-doped $BaTiO_3$/epoxy composites. Journal of the European Ceramic Society, 21, 1171-1177.

Lee, H.G., and Kim, H.G. (1990) Ceramic size dependence of dielectric and piezoelectric properties of piezoelectric ceramic-polymer composites. Journal of Applied Physics, 67(4), 2024-2028.

Liang, A., Chong, S.R., and Giannelis, E.P. (1998) Barium titanate/epoxy composite dielectric materials for integrated thin film capacitors. Electronic Components and Technology Conference, 171-175.

Liou, J.W., and Chiou, B.S. (1998) Dielectric tenability of barium strontium titanate/silicone-rubber composite. Journal of Physics: Condense Matter, 10, 2773-2786.

Li, X., Peng, Z., Fan, W., Wang, X., and Guo, K. (1997) Investigation on the properties of dielectric and incomplete molecules of nanocrystalline $BaTiO_3$ with cubic perovskite structure. Materials Chemistry and Physics, 47, 46-50.

Merz, W.J. (1949) The electric and optical behavior of $BaTiO_3$ single-domain crystal. Physical Review, 76(8), 1221-1225.

Merz, W.J. (1953) The Double hysteresis loop of $BaTiO_3$ at the Curie point. Physical Review, 91(3), 513-517.

Nair, C.P.R. (2004) Advances in addition-cure phenolic resins. Progress in polymer science, 29, 401-498.

Ning, X., and Ishida, H. (1994) Phenolic materials via ring-opening polymerization: synthesis and characterization of bisphenol-A-phenol benzoxazines and their polymers. Journal of Polymer Science, 32, 1121-1129.

Popielarz, R., Chiang, C.K., Nozaki, R., and Obrzut, J. (2001) Dielectric properties of polymer/ferroelectric ceramic composites from 100 Hz to 10 GHz. Macromolecules, 34, 5910-5915.

Rao, Y. and Wong, C. P. (2003) Material characterization of a high-dielectric constant polymer-ceramic composite for embedded capacitor applications. Journal of Applied Polymer Science, 36, 2228-2231.

Rao, Y., Takahashi, A., and Wong, C. P. (2003) Di-block copolymer study to optimize filler dispersion in high dielectric constant polymer-ceramic composite. Composite: Part A, 34, 1113-1116.

Safari, A. (1994) Development of piezoelectric composites for transducers. Journal of Physics III France, 4, 1129-1149.

Shen, S.B., and Ishida, H. (1999) Development and characterization of high performance polybenzoxazine composites. Polymer Composites, 17(5), 710-719.

Shen, S.B., and Ishida, H. (1999) Dynamic mechanical and thermal characterization of high-performance polybenzoxazine. Journal of Polymer Science: Part B, 37, 3257-3268.

Swartz, S.L. (1990) Topic in electronic ceramics. IEEE Transactions on Electrical Insulation, 25(5), 935-987.

Su, B., Holmes, J.E., Cheng, B.L., and Button, T.W. (2002) Processing effect of the microstructure and dielectric properties of barium strontium titanate (BST) ceramics. Journal of Electroceramics, 9, 111-116.

Tangwiwat, S. and Milne, S. J. (2005) Barium titanate sols prepared by a diol-based sol-gel route. Journal of Non-Crystalline Solids, 351, 976-980.

Wu, L., Chen, Y.C., Huang, C.Y., Chou, Y.P., and Tsai, Y.T. (2000) Direct-current field dependence of dielectric properties in alumina-doped barium strontium titanate. Journal of the American Ceramic Society, 83(7), 1713-1719.

Xie, S.H., Zhu, B.K., Wei, X.Z., Xu, Z.K., and Xu, Y.Y. (2005) Polyimide/$BaTiO_3$ composites with controllable dielectric properties. Composites: Part A, 36, 1152-1157.

Yang, W., Chang, A., and Yang, B. (2002) Preparation of barium strontium titanate ceramic by sol-gel method and microwave sintering. Journal of Materials Synthesis and Processing, 10(6), 303-309.

APPENDICES

Appendix A Lattice Parameter Calculation

The lattice parameter of unit cell $Ba_{1-x}Sr_xTiO_3$ were calculated as follow; the equation

Bragg's law $$n\lambda = 2d\sin\theta \quad \text{(A1)}$$

$$\lambda = 2d\sin\theta \quad (n=1) \quad \text{(A2)}$$

Cubic: $$\frac{1}{d^2} = \frac{(h^2+k^2+l^2)}{a^2} \quad \text{(A3)}$$

Tetragonal: $$\frac{1}{d^2} = \frac{(h^2+k^2)}{a^2} + \frac{l^2}{c^2} \quad \text{(A4)}$$

From equation (A2), we can write that

$$d^2 = \frac{\lambda^2}{4\sin^2\theta} \quad \text{(A5)}$$

Substitution of equation (A5) in equation (A3) and (A4), one obtains

Cubic: $$\sin^2\theta = \frac{\lambda^2}{4a^2}(h^2+k^2+l^2) \quad \text{(A6)}$$

Tetragonal: $$\sin^2\theta = \frac{\lambda^2(h^2+k^2)}{4a^2} + \frac{\lambda^2 l^2}{4c^2} \quad \text{(A7)}$$

We define $(h^2+k^2+l^2) = S$, where S is 1, 2, 3, 4, 5, and 6 for the cubic phase and $\lambda^2/4a^2$ is a constant. For tetragonal structure, $\lambda^2/4a^2$ and $\lambda^2/4c^2$ are both constant A and C. h^2+k^2 is 1, 2, 4, 5, and 8. Table A1-A6 show the lattice parameter of $BaTiO_3$ titanate calcined at different temperatures (600-1100°C). Table A7-A9 show the lattice parameter of $Ba_{1-x}Sr_xTiO_3$ with x = 0.3, 0.5, and 0.7 calcined at 800°C. Table A10-A13 show the lattice parameter of $Ba_{1-x}Sr_xTiO_3$ ceramics with x = 0, 0.3, 0.5, and 0.7.

Table A1 The identification of XRD peaks analyzed of cubic $BaTiO_3$ calcined at 600°C

2θ	θ	*hkl*	*S*	$\sin^2\theta$	$\lambda^2/4a^2$	*a* (Å)
22.05	11.02	100	1	0.0366	0.0366	4.0261
31.43	15.71	110	2	0.0735	0.0367	4.0207
38.79	19.39	111	3	0.1105	0.0368	4.0147
45.03	22.52	200	4	0.1472	0.0368	4.0173
50.74	25.37	210	5	0.1837	0.0367	4.0201
56.02	28.01	211	6	0.2216	0.0369	4.0099
65.70	32.85	220	8	0.2945	0.0368	4.0166
					a_{avg}	4.0206
					SD	0.0042

Table A2 The identification of XRD peaks analyzed of cubic $BaTiO_3$ calcined at 700°C

2θ	θ	*hkl*	*S*	$\sin^2\theta$	$\lambda^2/4a^2$	*a* (Å)
22.10	11.05	100	1	0.0368	0.0368	4.0182
31.48	15.74	110	2	0.0736	0.0368	4.0161
38.84	19.42	111	3	0.1106	0.0369	4.0127
45.15	22.57	200	4	0.1475	0.0369	4.0131
50.84	25.42	210	5	0.1844	0.0369	4.0126
56.11	28.06	211	6	0.2213	0.0370	4.0114
65.79	32.90	220	8	0.2952	0.0369	4.0115
					a_{avg}	4.0137
					SD	0.0025

Table A3 The identification of XRD peaks analyzed of cubic $BaTiO_3$ calcined at 800°C

2θ	θ	*hkl*	*S*	$\sin^2\theta$	$\lambda^2/4a^2$	*a* (Å)
22.12	11.06	100	1	0.0368	0.0368	4.0153
31.52	15.76	110	2	0.0738	0.0369	4.0111
38.80	19.40	111	3	0.1104	0.0368	4.0161
45.20	22.60	200	4	0.1478	0.0370	4.0085
50.90	25.45	210	5	0.1848	0.0370	4.0083
56.18	28.09	211	6	0.2219	0.0370	4.0072
65.87	32.94	220	8	0.2958	0.0370	4.0072
					a_{avg}	4.011
					SD	0.0037

Table A4 The identification of XRD peaks analyzed of tetragonal $BaTiO_3$ calcined at 900°C

2θ	θ	*hkl*	$\sin^2\theta$	$\sin^2\theta$ / 2	$\sin^2\theta$ / 4	$\sin^2\theta$ / 5	$\sin^2\theta$ / 8
22.16	11.08	100	0.0370				
31.53	15.76	110		0.0369			
45.34	22.67	200			0.0372		
51.01	25.50	210				0.0371	
65.84	32.92	220					0.0369

2θ	θ	*hkl*	$\sin^2\theta$	$\sin^2\theta$ / 2	$\sin^2\theta$ / 4	$\sin^2\theta$ / 5	$\sin^2\theta$ / 8
22.03	11.02	001	0.0365				
31.51	15.76	101		0.0368			
38.90	19.45	111			0.0369		
45.18	22.59	002	0.1476				
50.90	25.45	201				0.0367	
56.15	28.08	112			0.1476		
56.27	28.14	211					0.0374
65.77	32.88	202				0.1469	

$A = \lambda^2/4a^2$	a (Å)
0.0370	4.0075
0.0369	4.0095
0.0372	3.9967
0.0371	4.0001
0.0369	4.0088
a_{avg}	4.0045 ± 0.0058

$C = \lambda^2/4c^2$	c (Å)
0.0365	4.0311
0.0368	4.0188
0.0369	4.0114
0.0367	4.0212
0.0374	3.9842
0.0369	4.0107
0.0369	4.0109
0.0367	4.0211
c_{avg}	4.0137 ± 0.0138

Table A5 The identification of XRD peaks analyzed of tetragonal $BaTiO_3$ calcined at 1000°C

2θ	θ	*hkl*	$\sin^2\theta$	$\sin^2\theta / 2$	$\sin^2\theta / 4$	$\sin^2\theta / 5$	$\sin^2\theta / 8$
22.21	11.10	100	0.0371				
31.53	15.77	110		0.0369			
45.37	22.68	200			0.0372		
51.08	25.54	210				0.0372	
65.97	32.98	220					0.0371

2θ	θ	*hkl*	$\sin^2\theta$	$\sin^2\theta\text{-}A$	$\sin^2\theta\text{-}2A$	$\sin^2\theta\text{-}4A$	$\sin^2\theta\text{-}5A$
22.00	11.00	001	0.0364				
31.51	15.76	101		0.0367			
38.90	19.45	111			0.0367		
45.17	22.58	002	0.1476				
50.74	25.37	102		0.1466			
50.97	25.49	201				0.0368	
56.19	28.10	112			0.1477		
56.28	28.14	211					0.0370

$A = \lambda^2/4a^2$	a (Å)
0.0371	3.9990
0.0369	4.0088
0.0372	3.9948
0.0372	3.9945
0.0371	4.0019
a_{avg}	3.9998 ± 0.0059

$C = \lambda^2/4c^2$	c (Å)
0.0364	4.0361
0.0367	4.0236
0.0367	4.0210
0.0368	4.0144
0.0370	4.0056
0.0369	4.0115
0.0367	4.0248
0.0369	4.0093
c_{avg}	4.0193 ± 0.0098

Table A6 The identification of XRD peaks analyzed of tetragonal $BaTiO_3$ calcined at 1100°C

2θ	θ	*hkl*	$\sin^2\theta$	$\sin^2\theta$ / 2	$\sin^2\theta$ / 4	$\sin^2\theta$ / 5	$\sin^2\theta$ / 8
22.22	11.11	100	0.0372				
31.59	15.80	110		0.0371			
45.39	22.70	200			0.0372		
51.11	25.55	210				0.0372	
66.12	33.06	220					0.0372

2θ	θ	*hkl*	$\sin^2\theta$	$\sin^2\theta$-A	$\sin^2\theta$-$2A$	$\sin^2\theta$-$4A$	$\sin^2\theta$-$5A$
22.02	11.01	001	0.0365				
31.50	15.75	101		0.0366			
38.90	19.45	111			0.0366		
44.91	22.46	002	0.1460				
50.65	25.32	102		0.1459			
50.98	25.49	201				0.0367	
55.96	27.98	112			0.1460		
56.28	28.14	211					0.0368

$A = \lambda^2/4a^2$	a (Å)
0.0372	3.9973
0.0371	4.0019
0.0372	3.9927
0.0372	3.9928
0.0372	3.9936
a_{avg}	3.9956 ± 0.0040

$C = \lambda^2/4c^2$	c (Å)
0.0365	4.0340
0.0366	4.0295
0.0366	4.0267
0.0367	4.0241
0.0368	4.0192
0.0365	4.0330
0.0365	4.0345
0.0365	4.0337
0.0365	4.0323
c_{avg}	4.0297 ± 0.0053

Table A7 The identification of XRD peaks analysis of the sol-gel $Ba_{0.7}Sr_{0.3}TiO_3$ powders calcined at 800°C

2θ	θ	*hkl*	*S*	$\sin^2\theta$	$\lambda^2/4a^2$	*a* (Å)
22.34	11.17	100	1	0.0376	0.0376	3.9762
31.78	15.89	110	2	0.0750	0.0375	3.9787
39.18	19.59	111	3	0.1125	0.0375	3.9792
45.6	22.8	200	4	0.1503	0.0376	3.9755
51.32	25.66	210	5	0.1877	0.0375	3.9776
56.66	28.33	211	6	0.2254	0.0376	3.9760
66.44	33.22	220	8	0.3004	0.0375	3.9769
					a_{avg}	3.9772
					SD	0.0014

Table A8 The identification of XRD peaks analysis of the sol-gel $Ba_{0.5}Sr_{0.5}TiO_3$ powders calcined at 800°C

2θ	θ	*hkl*	*S*	$\sin^2\theta$	$\lambda^2/4a^2$	*a* (Å)
22.48	11.24	100	1	0.0380	0.0380	3.9518
31.96	15.98	110	2	0.0759	0.0379	3.9569
39.46	19.73	111	3	0.1141	0.0380	3.9521
45.92	22.96	200	4	0.1523	0.0381	3.9493
51.48	25.74	210	5	0.1887	0.0377	3.9661
57.00	28.50	211	6	0.2278	0.0380	3.9543
66.80	33.40	220	8	0.3032	0.0379	3.9580
					a_{avg}	3.9555
					SD	0.0056

Table A9 The identification of XRD peaks analysis of the sol-gel $Ba_{0.3}Sr_{0.7}TiO_3$ powders calcined at 800°C

2θ	θ	*hkl*	*S*	$\sin^2\theta$	$\lambda^2/4a^2$	a (Å)
22.6	11.3	100	1	0.0384	0.0384	3.9311
32.12	16.06	110	2	0.0766	0.0383	3.9377
39.62	19.81	111	3	0.1149	0.0383	3.9368
46.10	23.05	200	4	0.1534	0.0384	3.9348
51.86	25.93	210	5	0.1914	0.0383	3.9391
57.30	28.65	211	6	0.2300	0.0383	3.9354
67.24	33.62	220	8	0.3068	0.0383	3.9351
					a_{avg}	3.9357
					SD	0.0026

Table A10 The identification of XRD peaks analysis of the $BaTiO_3$ ceramic sintered at 1350°C

2θ	θ	*hkl*	$\sin^2\theta$	$\sin^2\theta$ / 2	$\sin^2\theta$ / 4	$\sin^2\theta$ / 5	$\sin^2\theta$ / 8
22.50	11.25	100	0.0381				
31.50	15.75	110		0.0369			
45.36	22.68	200			0.0372		
51.10	25.55	210				0.0372	
66.14	33.07	220					0.0372

2θ	θ	*hkl*	$\sin^2\theta$	$\sin^2\theta$-A	$\sin^2\theta$-2A	$\sin^2\theta$-4A	$\sin^2\theta$-5A
31.50	15.75	101	0.0737	0.0364			
38.88	19.44	111	0.1109		0.0362		
50.64	25.32	102	0.1830	0.1457			
50.98	25.49	201	0.1853			0.0360	
55.96	27.98	112	0.2203		0.1456		
56.28	28.14	211	0.2226				0.0360
65.74	32.87	202	0.2948			0.1455	

$A = \lambda^2/4a^2$	a (Å)
0.0381	3.9481
0.0369	4.0130
0.0372	3.9953
0.0372	3.9934
0.0372	3.9927
a_{avg}	3.9885 ±0.0241

$C = \lambda^2/4c^2$	c (Å)
0.0364	4.0382
0.0362	4.0498
0.0360	4.0591
0.0360	4.0632
0.0364	4.0372
0.0364	4.0384
0.0364	4.0407
c_{avg}	4.0467 ±0.0108

Table A11 The identification of XRD peaks analysis of the $Ba_{0.7}Sr_{0.3}TiO_3$ ceramic sintered at 1350°C

2θ	θ	*hkl*	$\sin^2\theta$	$\sin^2\theta / 2$	$\sin^2\theta / 4$	$\sin^2\theta / 5$	$\sin^2\theta / 8$
22.36	11.18	100	0.0376				
31.81	15.91	110		0.0376			
45.61	22.81	200			0.0376		
51.40	25.70	210				0.0376	
66.54	33.27	220					0.0376

2θ	θ	*hkl*	$\sin^2\theta$	$\sin^2\theta$-A	$\sin^2\theta$-$2A$	$\sin^2\theta$-$4A$	$\sin^2\theta$-$5A$
22.32	11.16	001	0.0375				
39.24	19.62	111			0.0376		
45.61	22.81	002	0.1504				
56.71	28.35	112			0.1505		
56.82	28.41	211					0.0384
66.47	33.24	202				0.1502	

$A = \lambda^2/4a^2$	a (Å)
0.03763	3.9724
0.03759	3.9744
0.03759	3.9744
0.03764	3.9714
0.03764	3.9716
a_{avg}	3.9728 ± 0.0015

$C = \lambda^2/4c^2$	c (Å)
0.0375	3.9794
0.0376	3.9746
0.0376	3.9744
0.0376	3.9730
0.0376	3.9733
0.0375	3.9771
c_{avg}	3.9745 ± 0.0025

Table A12 The identification of XRD peaks analysis of the $Ba_{0.5}Sr_{0.5}TiO_3$ ceramic sintered at 1350°C

2θ	θ	*hkl*	*S*	$\sin^2\theta$	$\lambda^2/4a^2$	a (Å)
22.44	11.22	100	1	0.0379	0.0379	3.9583
31.99	15.99	110	2	0.0760	0.0380	3.9534
39.46	19.73	111	3	0.1141	0.0380	3.9517
45.91	22.95	200	4	0.1522	0.0380	3.9503
51.70	25.85	210	5	0.1903	0.0381	3.9499
57.07	28.54	211	6	0.2284	0.0381	3.9495
66.97	33.48	220	8	0.3046	0.0381	3.9491
					a_{avg}	3.9517
					SD	0.0032

Table A13 The identification of XRD peaks analysis of the $Ba_{0.3}Sr_{0.7}TiO_3$ ceramic sintered at 1350°C

2θ	θ	*hkl*	*S*	$\sin^2\theta$	$\lambda^2/4a^2$	*a* (Å)
22.56	11.28	100	1	0.0383	0.0383	3.9382
32.15	16.07	110	2	0.0767	0.0384	3.9342
39.66	19.83	111	3	0.1152	0.0384	3.9329
46.13	23.07	200	4	0.1536	0.0384	3.9317
51.96	25.98	210	5	0.1920	0.0384	3.9319
57.36	28.68	211	6	0.2305	0.0384	3.9314
67.32	33.66	220	8	0.3074	0.0384	3.9309
					a_{avg}	3.9330
					SD	0.0025

Appendix B SEM Micrographs of Sol-Gel $Ba_{1-x}Sr_xTiO_3$ Powders

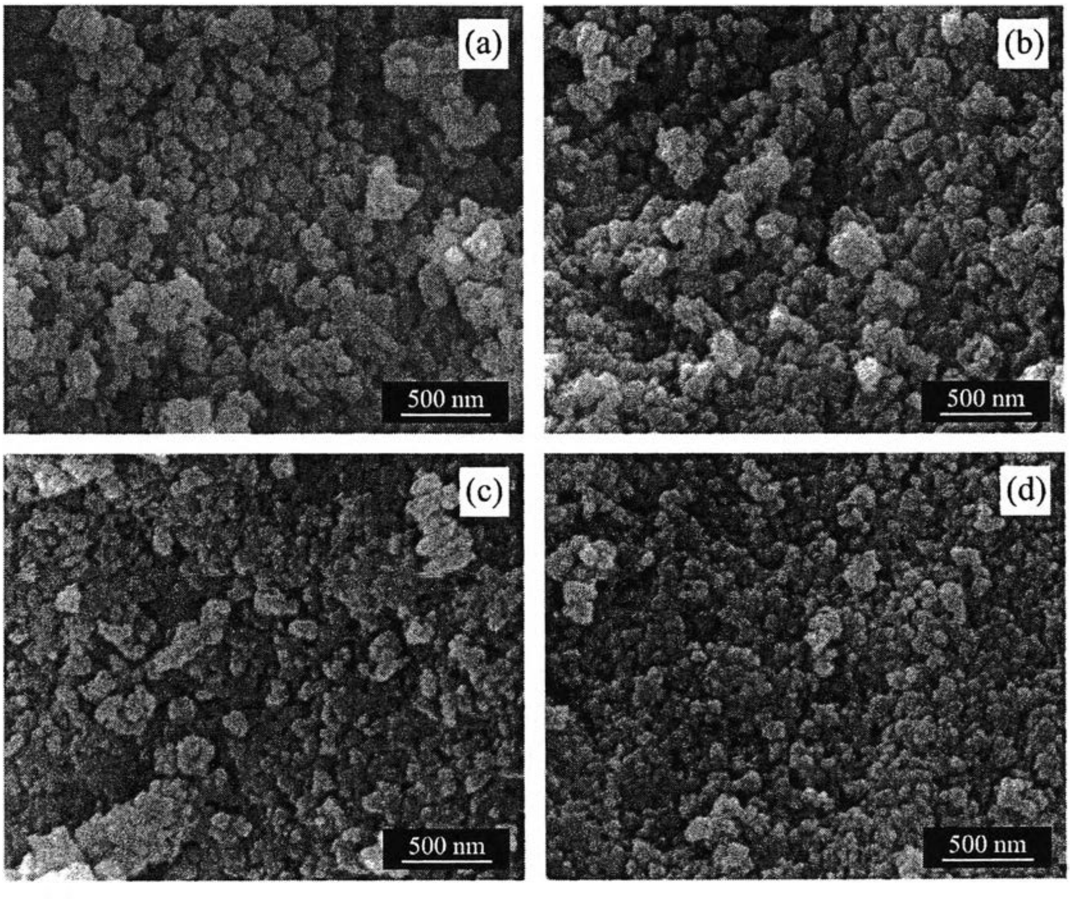

Figure B1 SEM micrographs of sol-gel $Ba_{1-x}Sr_xTiO_3$ powders calcined at 800 °C for 80 min; (a) $x = 0$, (b) $x = 0.3$, (c) $x = 0.5$, and (d) $x = 0.7$.

Appendix C The Dielectric Constant and Loss tangent at Different Frequencies

Table C1 The dielectric constant of SG-BT/polybenzoxazine composites

Materials	Frequency (Hz)				
	10^3	10^4	10^5	10^6	10^7
PBZZ	3.81	3.72	3.64	3.58	3.56
30 wt% SG-BT (9 vol%)	5.71	5.57	5.47	5.34	5.29
40 wt% SG-BT (12 vol%)	7.07	6.82	7.86	6.43	6.31
50 wt% SG-BT (18 vol%)	8.48	8.14	9.09	7.65	7.52
60 wt% SG-BT (25 vol%)	9.67	9.35	13.47	8.88	8.76
70 wt% SG-BT (34 vol%)	14.09	13.77	13.47	13.22	13.16

Table C2 The dielectric constant of ST-BT/polybenzoxazine composites

Materials	Frequency (Hz)				
	10^3	10^4	10^5	10^6	10^7
30 wt% ST-BT (8 vol%)	4.86	4.54	4.31	4.23	4.11
40 wt% ST-BT (12 vol%)	6.36	5.62	5.19	4.86	4.31
50 wt% ST-BT (17 vol%)	8.80	8.21	7.72	7.37	7.11
60 wt% ST-BT (22 vol%)	11.57	10.76	10.01	9.41	9.00
70 wt% ST-BT (30 vol%)	13.76	12.92	12.27	11.73	11.29

Table C3 The dielectric constant of SG-BST/polybenzoxazine composites

Materials	Frequency (Hz)				
	10^3	10^4	10^5	10^6	10^7
30 wt% SG-BST (10 vol%)	7.10	6.93	6.68	6.45	6.34
40 wt% SG-BST (15 vol%)	7.96	7.63	7.28	7.01	6.84
50 wt% SG-BST (20 vol%)	10.09	9.72	9.38	9.10	8.83
60 wt% SG-BST (25 vol%)	12.54	12.08	11.68	11.34	10.99
70 wt% SG-BST (38 vol%)	17.51	16.98	16.43	16.02	15.90
80 wt% SG-BST (48 vol%)	28.03	27.17	27.17	26.50	25.47

Table C4 The loss tangent of SG-BT/polybenzoxazine composites

Materials	Frequency (Hz)				
	10^3	10^4	10^5	10^6	10^7
PBZZ	0.0149	0.0159	0.0126	0.0126	0.0120
30 wt% SG-BT (9 vol%)	0.0365	0.0319	0.0290	0.0244	0.0341
40 wt% SG-BT (12 vol%)	0.0249	0.0226	0.0227	0.0176	0.0154
50 wt% SG-BT (18 vol%)	0.0232	0.02329	0.0224	0.0171	0.0220
60 wt% SG-BT (25 vol%)	0.0282	0.0213	0.0197	0.0148	0.0179
70 wt% SG-BT (34 vol%)	0.0334	0.0314	0.0181	0.0227	0.0238

Table C5 The loss tangent of ST-BT/polybenzoxazine composites

Materials	Frequency (Hz)				
	10^3	10^4	10^5	10^6	10^7
30 wt% ST-BT (8 vol%)	0.0392	0.0350	0.0283	0.0266	0.0321
40 wt% ST-BT (12 vol%)	0.0439	0.0355	0.0330	0.0254	0.0274
50 wt% ST-BT (17 vol%)	0.0495	0.0437	0.0372	0.0303	0.0338
60 wt% ST-BT (22 vol%)	0.0498	0.0490	0.0459	0.0395	0.0479
70 wt% ST-BT (30 vol%)	0.0445	0.0409	0.0324	0.0263	0.0296

Table C6 The loss tangent of SG-BST/polybenzoxazine composites

Materials	Frequency (Hz)				
	10^3	10^4	10^5	10^6	10^7
30 wt% SG-BST (8 vol%)	0.0365	0.0319	0.0319	0.0244	0.0341
40 wt% SG-BST (12 vol%)	0.0207	0.0218	0.0233	0.0267	0.0266
50 wt% SG-BST (17 vol%)	0.0166	0.0253	0.0241	0.0219	0.0393
60 wt% SG-BST (22 vol%)	0.0225	0.0230	0.0234	0.0228	0.0273
70 wt% SG-BST (38 vol%)	0.0217	0.0210	0.0200	0.0170	0.0294
80 wt% SG-BST (48 vol%)	0.0362	0.0189	0.0160	0.0171	0.0306

Table C7 The dielectric constant of $Ba_{1-x}Sr_xTiO_3$ (x = 0, 0.3, 0.5, and 0.7) ceramics

Materials	Frequency (Hz)					
	10^2	10^3	10^4	10^5	10^6	10^7
$BaTiO_3$	1362	1232	1145	1145	1100	233
$Ba_{0.7}Sr_{0.3}TiO_3$	2904	2795	2672	2672	2568	97
$Ba_{0.5}Sr_{0.5}TiO_3$	942	946	941	941	938	804
$Ba_{0.3}Sr_{0.7}TiO_3$	326	308	297	297	292	260

Table C8 The loss tangent of $Ba_{1-x}Sr_xTiO_3$ (x = 0, 0.3, 0.5, and 0.7) ceramics

Materials	Frequency (Hz)					
	10^2	10^3	10^4	10^5	10^6	10^7
$BaTiO_3$	0.1263	0.0675	0.0416	0.0349	0.1728	1.9786
$Ba_{0.7}Sr_{0.3}TiO_3$	0.0340	0.0316	0.0289	0.0506	0.2642	10.57
$Ba_{0.5}Sr_{0.5}TiO_3$	0.0086	0.0128	0.0032	0.0077	0.0565	0.7344
$Ba_{0.3}Sr_{0.7}TiO_3$	0.3570	0.0763	0.0224	0.0126	0.0451	0.4656

Appendix D Characterizations of Barium Titanate ($BaTiO_3$)/Polybenzoxazine Composites

Two ceramic-polymer composites were also fabricated and investigated. The ceramic fillers include sol-gel barium titanate powders (SG-BT) and sintered barium titanate powders (ST-BT). The densities of composites were measured as function of ceramic content. For dielectric measurement, dielectric constant and loss tangent of composites were measured as function of ceramic volume fraction and frequency.

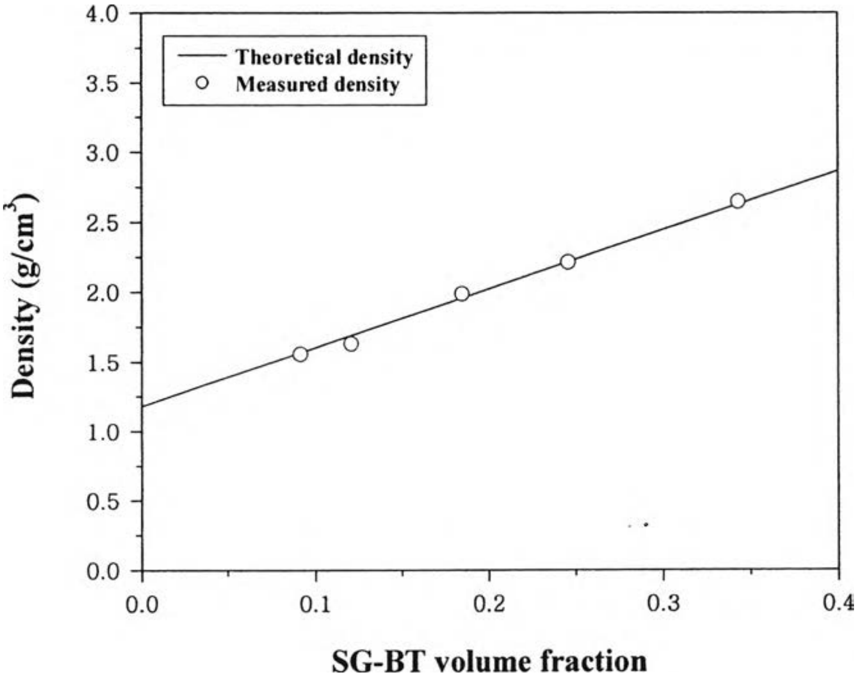

Figure D1 Comparison between measured density (◊) and theoretical density (—) as a function of SG-BT.

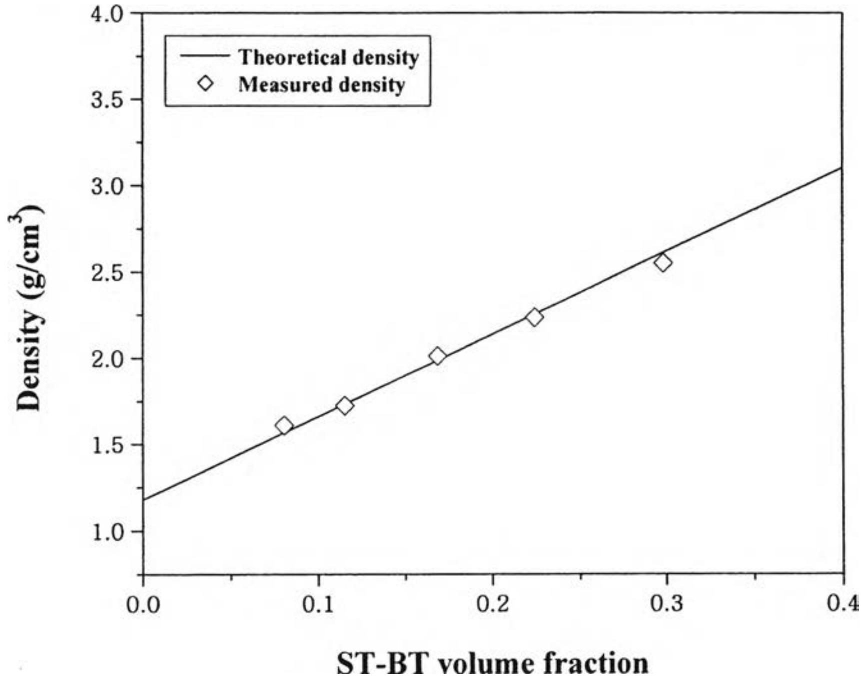

Figure D2 Comparison between measured density (◊) and theoretical density (—) as a function of ST-BT.

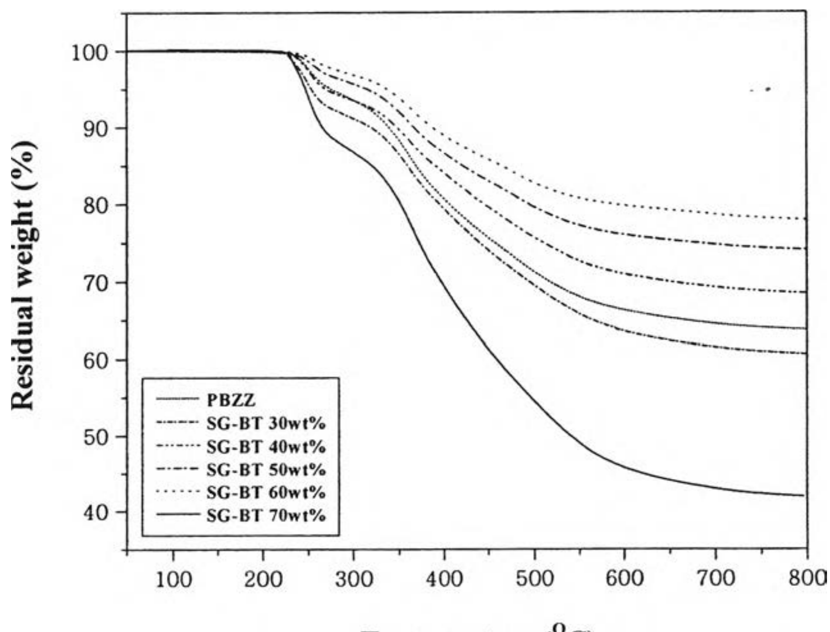

Figure D3 TGA curve of composites at different SG-BT content in nitrogen atmosphere.

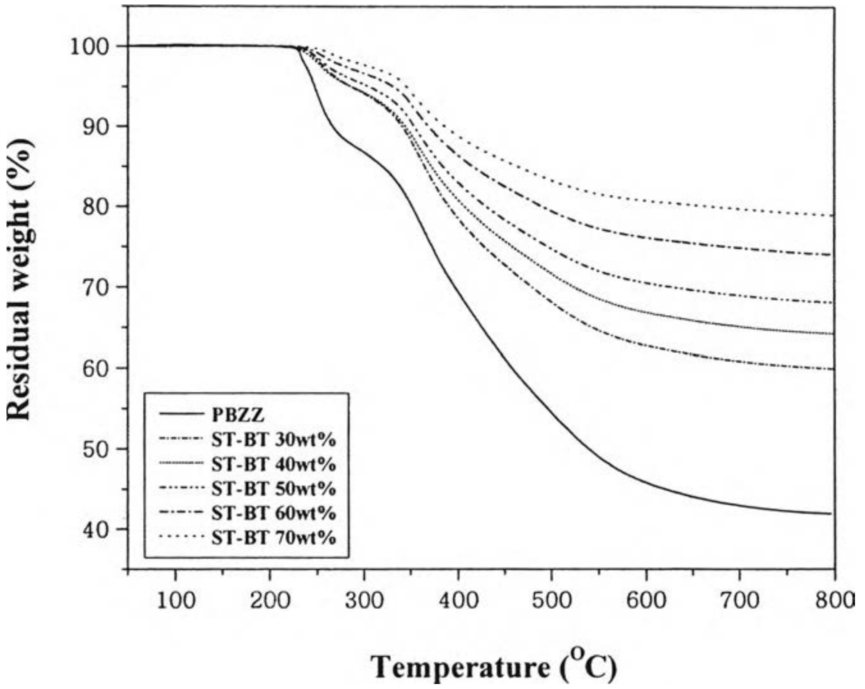

Figure D4 TGA curve of composites at different ST-BT contents in nitrogen atmosphere.

Table D1 Properties of the composite at various SG-BT contents

Composites	Volume fraction	Density (g/cm^3)	Residual weight% at 800°C
PBZZ/SG-BT 30 wt%	0.09	1.55	60.54
PBZZ/SG-BT 40 wt%	0.12	1.63	63.69
PBZZ/SG-BT 50 wt%	0.18	1.99	68.44
PBZZ/SG-BT 60 wt%	0.25	2.21	74.06
PBZZ/SG-BT 70 wt%	0.34	2.64	77.91

Table D2 Properties of the composites at various ST-BT contents

Composites	Volume fraction	Density (g/cm^3)	Residual weight% at 800°C
PBZZ/ST-BT 30 wt%	0.08	1.61	59.93
PBZZ/ST-BT 40 wt%	0.11	1.72	64.24
PBZZ/ST-BT 50 wt%	0.17	2.01	68.12
PBZZ/ST-BT 60 wt%	0.22	2.23	74.09
PBZZ/ST-BT 70 wt%	0.29	2.55	78.98

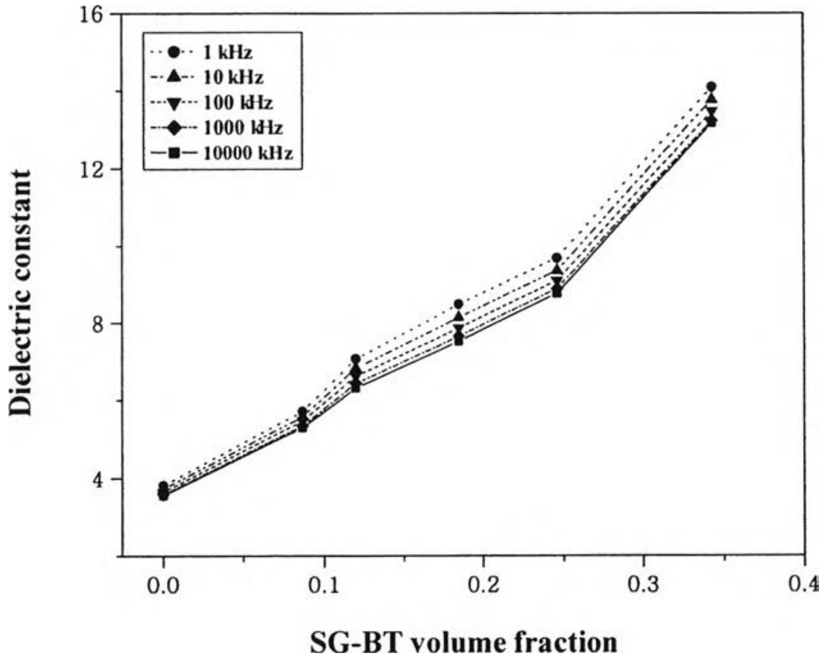

Figure D5 Dielectric constant of the composites at different SG-BT volume fraction and frequencies.

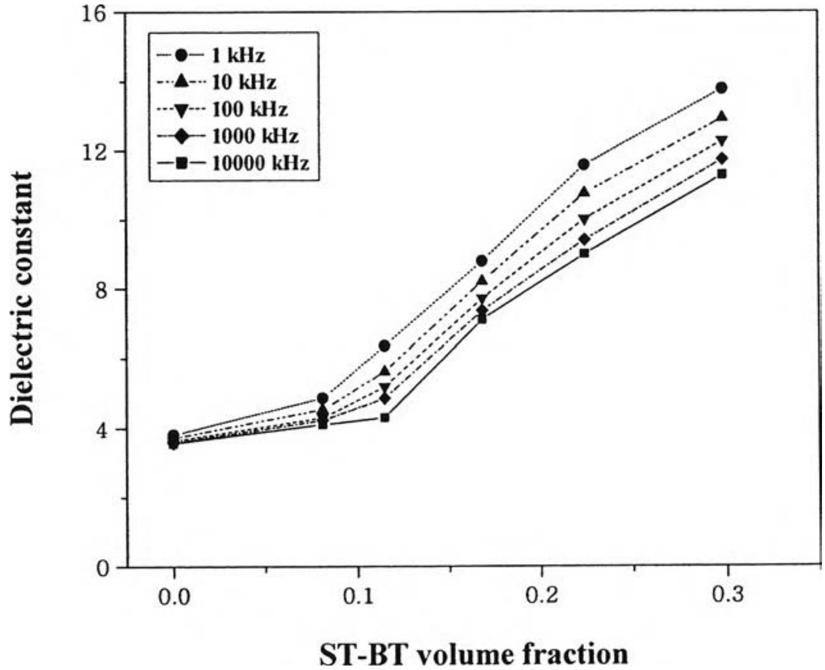

Figure D6 Dielectric constant of the composites at different ST-BT volume fraction and frequencies.

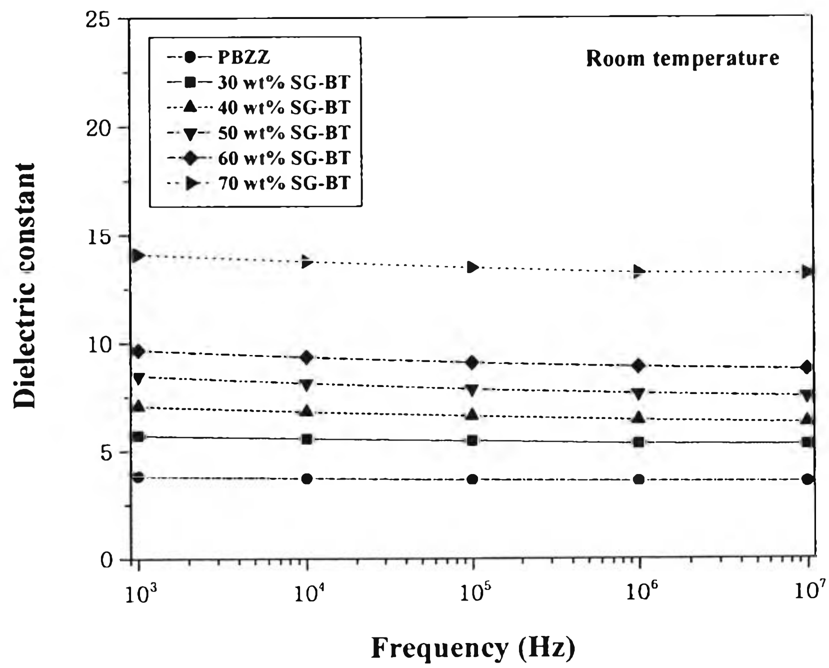

Figure D7 Frequency dependence of dielectric constant for the composites at various SG-BT contents.

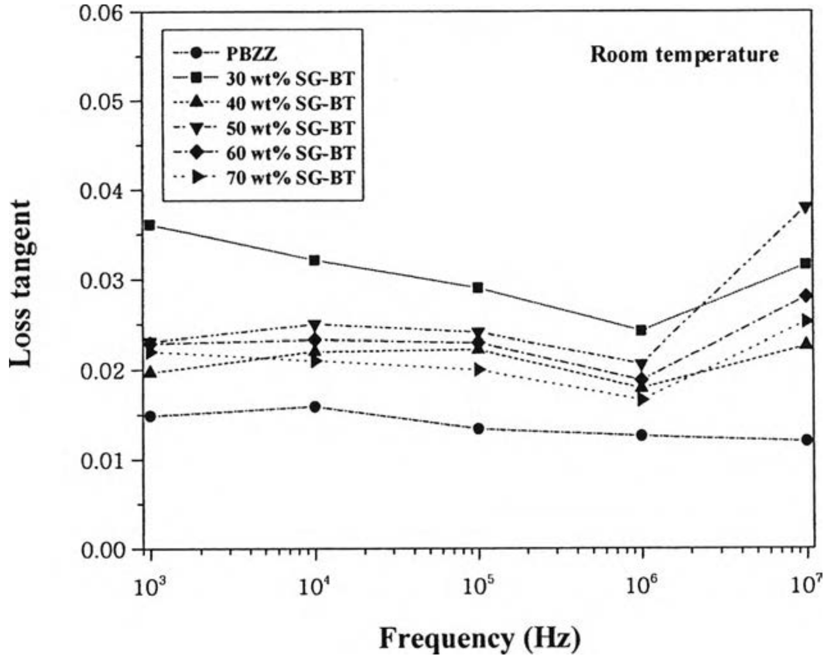

Figure D8 Frequency dependence of loss tangent for the composites at various SG-BT contents.

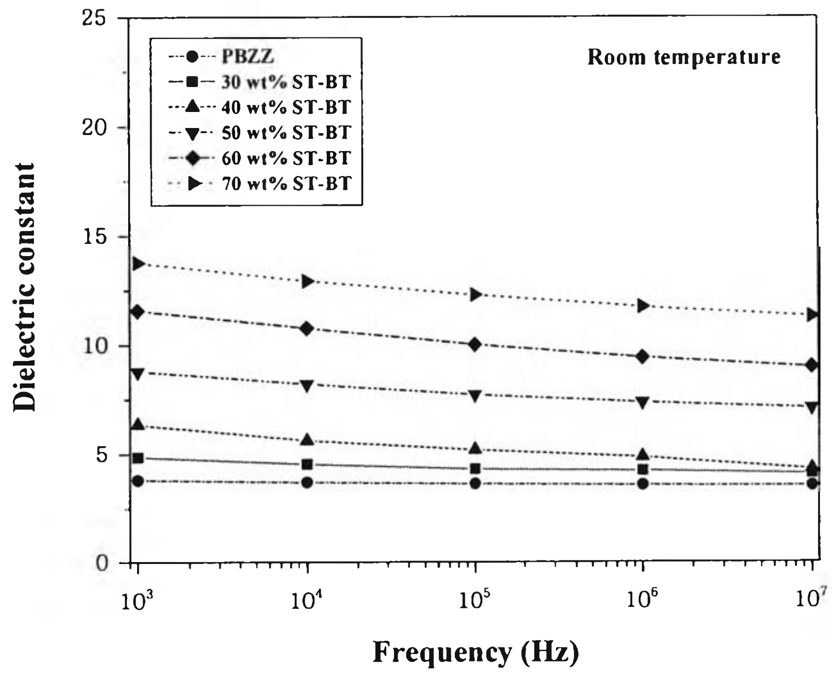

Figure D9 Frequency dependence of dielectric constant for the composites at various ST-BT contents.

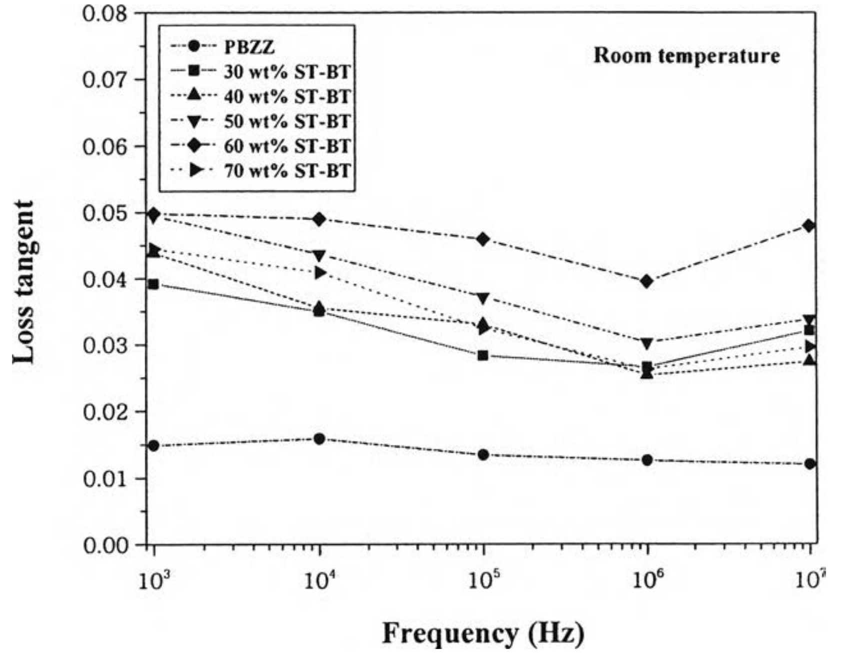

Figure D10 Frequency dependence of loss tangent of the composite at various ST-BT contents.

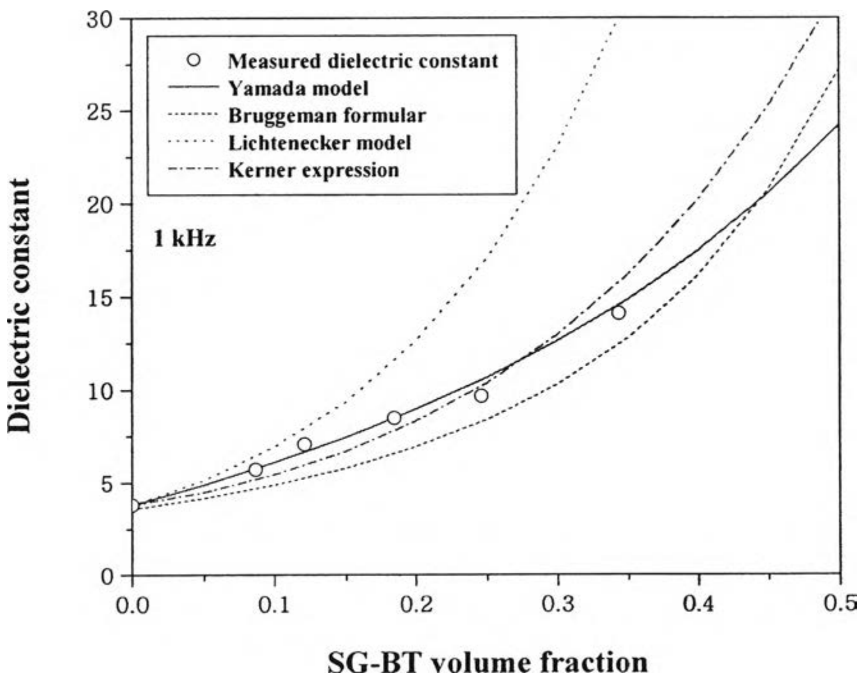

Figure D11 Plot of theoretical models and the measured dielectric constant for different SG-BT volume fractions at room temperature and 1 kHz.

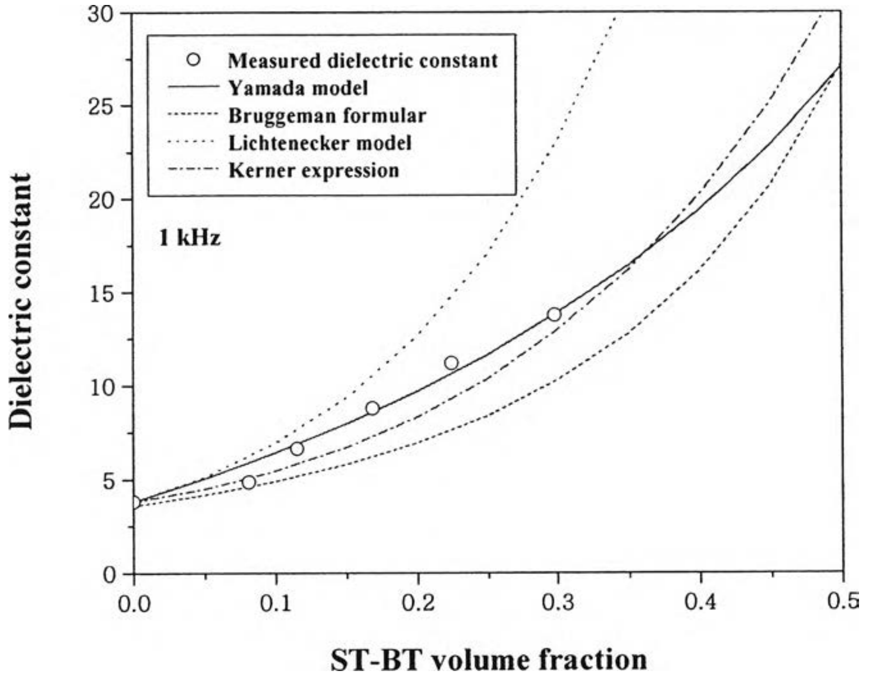

Figure D12 Plot of theoretical models and the measured dielectric constant for different ST-BT volume fractions at room temperature and 1 kHz.

Appendix E Shape Parameter

The shape parameter of the ellipsoid is the inverse of the depolarization factor in the field direction; that is

$$\frac{1}{\eta}=\frac{a^2c}{2}\int_0^\infty \frac{du}{(c^2+u^2)^{3/2}(a^2+u)} \tag{E1}$$

where a and c are the axis lengths of the ellipsoid perpendicular and parallel to the applied field. The axis ratio (from 0.1-4.5) versus the shape parameter are plotted in Figure E1 (Liou and Chiou, 1998).

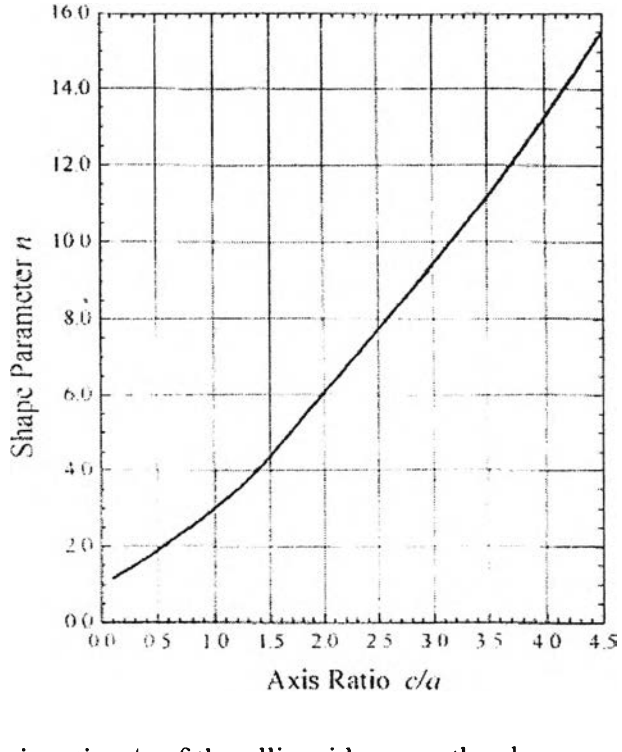

Figure E1 The axis ratio c/a of the ellipsoid versus the shape parameter η calculated from equation E1.

CURRICULUM VITAE

Name: Mr. Gasidit Panomsuwan

Date of Birth: September 8, 1983

Nationality: Thai

University Education:

2001-2005 Bachelor Degree of Science in Physics, Faculty of Science, Chulalongkorn University, Bangkok, Thailand

Presentations:

1. Panomsuwan, G., Ishida, I., and Manuspiya, H., (2006, December 10-14) A novel polymer-ceramic nanocomposite for embedded capacitor application. Paper presented at 5th Asian Meeting on Electroceramics, Bangkok, Thailand.
2. Panomsuwan, G., Ishida, I., and Manuspiya, H., (2007, January 16-19) Synthesis of polybenzoxazine and nano-barium titanate for a novel composite. Paper presented at 2nd IEEE Nano/micro Engineered and Molecular Systems 2007, Bangkok, Thailand.
3. Panomsuwan, G., Ishida, I., and Manuspiya, H., (2007, April 13-16) Dielectric properties of barium (strontium) titanate/polybenzoxazine composite with 0-3 connectivity. Paper presented at Material Research Society: Spring 2007, San Francisco, USA.